

# Sympathetic cooling of fluorine atoms with ultracold atomic hydrogen

Maykel L. González-Martínez\* and Jeremy M. Hutson†

*Joint Quantum Centre (JQC) Durham/Newcastle, Department of Chemistry,  
Durham University, South Road, Durham DH1 3LE, United Kingdom*

(Dated: November 14, 2018)

We consider the prospect of using ultracold hydrogen atoms for sympathetic cooling of fluorine atoms to microkelvin temperatures. We carry out quantum-mechanical calculations on collisions between cold F and H atoms in magnetically trappable states and show that the ratio of elastic to inelastic cross sections remains high across a wide range of temperatures and magnetic fields. For F atoms initially in the spin-stretched state ( $^2P_{3/2}$ ,  $f = m_f = +2$ ), sympathetic cooling appears likely to succeed from starting temperatures around 1 K or even higher. This occurs because inelastic collisions are suppressed by p-wave and d-wave barriers that are 600 mK and 3.2 K high, respectively. In combination with recent results on H + NH and H + OH collisions [M. L. González-Martínez and J. M. Hutson, arXiv:1305.6282 (2013)], this establishes ultracold H atoms as a very promising and versatile coolant for atoms and molecules that cannot be laser-cooled.

PACS numbers: 37.10.De, 34.50.Cx

## I. INTRODUCTION

Reaching the *cold* ( $T < 1$  K) and *ultracold* ( $T < 1$  mK) regimes has triggered the revival of atomic physics. In less than two decades, it has led to the creation of Bose-Einstein condensates (BEC) [1–3] and Fermi degenerate gases [4, 5], atom lasers [6], quantized vortices [7], solitons [8, 9], and optical lattices [10]. It has had a significant impact in high-precision measurement and in the study of collective phenomena such as superfluidity and superconductivity [11–13]. In addition, it has opened up the possibility of full control of atomic interactions and scattering properties using external fields [14].

The atoms that can currently be cooled to the ultracold regime form only a small part of the periodic table. They include alkali metals, some alkaline earths, and relatively exotic species such as Yb, Cr, Dy, Er and metastable He, all of which are amenable to laser Doppler cooling. However, there are many other atoms that cannot yet be cooled to such temperatures, including chemically important elements such as carbon, nitrogen, oxygen and the halogens. Halogen atoms are particularly interesting; they are reactive species that are often used as prototypes in the study of chemical reaction dynamics, and ultracold halogen atoms would offer fascinating possibilities for exploring chemical reactions in the cold and ultracold regime [15, 16].

Laser cooling of halogen atoms is not currently possible, since the UV lasers needed to excite their lowest one-photon transitions are not available. However, Doherty *et al.* [17] have recently used the PhotoStop approach [18] to trap Br atoms below 1 K at number densities up to  $10^8$  cm $^{-3}$ . In addition, halogen atoms may be amenable

to Zeeman deceleration [19]. However, such techniques by themselves are unlikely to reach the true ultracold regime below 1 mK and a second-stage cooling method is needed.

We have recently shown [20] that sympathetic cooling using spin-polarized ultracold atomic hydrogen offers a promising way to cool prototype molecules to the ultracold regime. For NH, our calculations suggested that sympathetic cooling with H atoms may be successful from a starting temperature of 1 K or even higher; this contrasts with sympathetic cooling with heavier atoms such as Li [21] or Mg [22, 23], which is predicted to succeed only if the molecules can be precooled to 10 or 20 mK. The general problem of sympathetic cooling for species in electric [24] or magnetic traps [25] is that static traps can confine species only when they are in *low-field-seeking* states, and these states are never the lowest state in the applied field. Collisions that transfer atoms or molecules to the lower states release kinetic energy and usually eject both collision partners from the trap. The key quantity that determines the feasibility of sympathetic cooling is the ratio  $\gamma$  between the cross-section for elastic collisions (which produce thermalization) and that for inelastic collisions (which cause trap loss). A common rule of thumb is that, for cooling to be successful, this ratio needs to be at least 100 [26].

In this paper we explore the use of sympathetic cooling with ultracold hydrogen atoms for fluorine atoms in their ground state,  $^2P_{3/2}$ . We have modified the MOLSCAT package [27, 28] to carry out quantum collision calculations between H and F atoms in a magnetic field, including hyperfine interactions for both H and F. The H+F system is simple enough that we can fully include all the potential curves that can contribute, including the deeply bound  $^1\Sigma^+$  ground state of HF, and also take full account of hyperfine structure.

\* Present address: Laboratoire Aimé Cotton, CNRS, Université Paris-Sud XI, ENS Cachan, Bât. 505, Campus d'Orsay, 91405 Orsay, France; maykel.gonzalez-martinez@u-psud.fr

† J.M.Hutson@durham.ac.uk

## II. THEORY

### A. Collision Hamiltonian

In this section we describe the general theory for collisions between an atom A in a  $2s_1+1S$  state and an atom B in a state with orbital angular momentum  $l_2$  and electron spin  $s_2$  in the presence of an external magnetic field. We follow the convention of using lower-case letters for operators and quantum numbers for the individual atoms, and capital letters for those of the collision complex as a whole. The vector  $\mathbf{R}$  joins the centers of mass of the atoms, while  $\mathbf{u}_r$  represents a unit vector conjugate to the orbital angular momentum of atom B. Where necessary, subscripts 1 and 2 refer to atoms A and B, respectively.

We solve the time-independent Schrödinger equation for the scattering wave function  $\Psi$  at energy  $E$ ,  $\hat{H}\Psi = E\Psi$ . The collision Hamiltonian may be written

$$\hat{H} = -\frac{\hbar^2}{2\mu}R^{-1}\frac{d^2}{dR^2}R + \frac{\hbar^2\hat{L}^2}{2\mu R^2} + \hat{H}_1 + \hat{H}_2 + \hat{H}_{12}, \quad (1)$$

where  $R$  is the internuclear distance,  $\hat{L}$  is the space-fixed operator for the end-over-end rotation and  $\mu$  is the reduced mass for the collision.  $\hat{H}_1$  and  $\hat{H}_2$  describe the separated atoms, while  $\hat{H}_{12}$  describes the interaction between them, with contributions that include both the electronic potential  $\hat{V}$  and the dipolar interaction  $\hat{H}_{\text{dip}}$  between the magnetic moments of the two atoms.

In the general case of non-zero electronic and nuclear spins, the Hamiltonian for an isolated atom B in a state  $2s_2+1l_2$  can be decomposed into spin-orbit, hyperfine and Zeeman contributions,

$$\hat{H}_2 = \hat{H}_{\text{so}} + \hat{H}_{\text{hf},2} + \hat{H}_{\text{Z},2}. \quad (2)$$

In Russell-Saunders coupling, the spin-orbit term may be written  $\hat{H}_{\text{so}} = a_{\text{so}}\hat{l}_2 \cdot \hat{s}_2$ , where  $a_{\text{so}}$  is the spin-orbit constant, and  $\hat{l}_2$  and  $\hat{s}_2$  are the electronic orbital angular momentum and spin operators. Corrections to this are required to handle deviations from Russell-Saunders coupling [29].

The leading terms in  $\hat{H}_{\text{hf},2}$  are the magnetic dipole and electric quadrupole contributions. The magnetic dipole term may be written  $a_j\hat{i}_2 \cdot \hat{j}_2$ , where  $\hat{j}_2 = \hat{l}_2 + \hat{s}_2$  and the  $a_j$  are the associated coupling constants [30, 31]. The quadrupolar term (which exists only if  $i_2 \geq 1$ , so is not present for  $^1\text{H}$  or  $^{19}\text{F}$ ) may be written  $\hat{H}_{\text{Q}} = 2b_j\hat{i}_2 \cdot \hat{j}_2(2\hat{i}_2 \cdot \hat{j}_2 + 1)$  [30, 31].

Finally, the Zeeman term arises from the interaction of the atomic magnetic moment with the external magnetic field  $\mathbf{B}$ . It may be written  $\hat{H}_{\text{Z},2} = -\hat{\mu}_2 \cdot \mathbf{B}$ , where  $\hat{\mu}_2 = -g'_L\mu_B\hat{l}_2 - g_S\mu_B\hat{s}_2 + g_{i2}\mu_N\hat{i}_2$  [32],  $g'_L \approx 1$ ,  $g_S \approx 2$  and  $g_{i2}$  are the ‘corrected’ orbital [33], electron and nuclear  $g$ -factors, and  $\mu_B$  and  $\mu_N$  are the Bohr and nuclear magnetons.

The Hamiltonian for an isolated atom A in a  $2s_1+1S$  state is obtained from that for B by setting  $l_1 = 0$ ,

and contains hyperfine and Zeeman contributions only, so that  $\hat{H}_1 = \hat{H}_{\text{hf},1} + \hat{H}_{\text{Z},1}$ .  $\hat{H}_{\text{hf},1}$  reduces to the Fermi contact interaction  $\hat{H}_{\text{F},1} = b_{\text{F},1}\hat{s}_1 \cdot \hat{i}_1$ , with  $b_{\text{F},1}$  an effective coupling constant, and  $\hat{s}_1$  and  $\hat{i}_1$  the electronic and nuclear spin operators. The Zeeman term is the same as that for atom B, except that  $\hat{\mu}_1 = -g_S\mu_B\hat{s}_1 + g_{i1}\mu_N\hat{i}_1$ .

The general expansion for the electronic interaction potential between two atoms with arbitrary angular momentum has been derived by Krems, Groenenboom and Dalgarno [34]. First, since the operator for the total interaction potential  $\hat{V}(\mathbf{R}, \mathbf{u}_r)$  is diagonal in the total electronic spin  $S$  ( $\hat{S} = \hat{s}_1 + \hat{s}_2$ ) and its space-fixed projection  $M_S$ , it can be decomposed into contributions  $\hat{V}^S(\mathbf{R}, \mathbf{u}_r)$ ,

$$\hat{V}(\mathbf{R}, \mathbf{u}_r) = \sum_{S=|s_1-s_2|}^{s_1+s_2} \sum_{M_S=-S}^S |SM_S\rangle\langle SM_S| \hat{V}^S(\mathbf{R}, \mathbf{u}_r). \quad (3)$$

For interaction of an S-state atom A with an  $l_2$ -state atom B, there are  $l_2 + 1$  molecular electronic states for each  $S$  with projections  $|\Lambda| = 0, \dots, l_2$  onto the internuclear axis. In the approximation that  $l_2$  is conserved at all values of  $R$ , these potentials can be represented by an expansion in Legendre polynomials,

$$\hat{V}^S(\mathbf{R}, \mathbf{u}_r) = \sum_k \hat{V}_k^S(R) P_k(\mathbf{u}_R \cdot \mathbf{u}_r), \quad (4)$$

where  $k = 0, 2, \dots, 2l_2$ ,  $\mathbf{u}_R \equiv (\theta, \phi)$  is a unit vector in the direction of  $\mathbf{R}$ ,

$$\hat{V}_k^S(R) = \frac{(2k+1)}{(2l_2+1)} \sum_{\Lambda=-l_2}^{l_2} \frac{\langle l_2\Lambda k 0 | l_2\Lambda \rangle}{\langle l_2 0 k 0 | l_2 0 \rangle} \hat{V}_\Lambda^S(R), \quad (5)$$

and  $\langle j_1 m_1 j_2 m_2 | j m \rangle$  is a Clebsch-Gordan coefficient. For the specific case where atom B is a halogen,  $l_2 = 1$ , and Eq. (5) reduces to one isotropic ( $k = 0$ ) and one anisotropic ( $k = 2$ ) component for each  $S$ ,

$$\hat{V}_0^S(R) = \frac{1}{3} [\hat{V}_\Sigma^S(R) + 2\hat{V}_\Pi^S(R)], \quad (6)$$

$$\hat{V}_2^S(R) = \frac{5}{3} [\hat{V}_\Sigma^S(R) - \hat{V}_\Pi^S(R)]. \quad (7)$$

The direct dipolar interaction between the magnetic moments of the two atoms may be written [35]

$$\hat{H}_{\text{dip}} = -\sqrt{6}(\mu_0/4\pi)R^{-3}\mathbf{T}^2(\hat{\mu}_1, \hat{\mu}_2) \cdot \mathbf{T}^2(\mathbf{u}_R), \quad (8)$$

where  $\mu_0$  is the magnetic permeability of free space and  $\mathbf{T}^k$  represent a spherical tensor of rank  $k$ .

In the present work, we assume that all the atomic coupling constants are independent of the internuclear distance  $R$ . Any variation of these constants could be introduced as an additional term in the interaction operator  $\hat{H}_{12}$ , as has been done, for example, for the  $R$ -dependence of hyperfine interactions for the interactions between alkali-metal atoms and closed-shell atoms [36, 37]. Such effects might include, for example, the

distance-dependence of the spin-orbit coupling constant  $a_{\text{so}}$ , or a nuclear quadrupole interaction in atom A (if  $i_1 \geq 1$ ) as a result of the breakdown of its spherical symmetry when the two atoms approach one another.

### B. Coupled-channel equations

We solve the quantum-mechanical scattering problem using the coupled-channel method. The total wave function is first expanded in a set of  $N$  conveniently chosen basis functions  $|a\rangle$

$$\Psi(R, \xi) = R^{-1} \sum_a \chi_a(R) |a\rangle, \quad (9)$$

where  $\xi$  is a collective variable including all coordinates except  $R$ , and  $a$  is the set of quantum numbers that label the basis functions. Each different combination of quantum numbers  $a$  defines a *channel*. A set of coupled differential equations for the *channel functions*  $\chi_a(R)$  is then obtained by substituting  $\Psi(R, \xi)$  into the time-independent Schrödinger equation to yield,

$$\frac{d^2 \chi_a}{dR^2} = \sum_{a'} (W_{aa'} - \epsilon \delta_{aa'}) \chi_{a'}, \quad (10)$$

where  $\delta_{ij}$  is the Kronecker delta,  $\epsilon = 2\mu E/\hbar^2$  is a scaled energy and

$$W_{aa'}(R) = \frac{2\mu}{\hbar^2} \langle a | \hat{\mathcal{H}}_1 + \hat{\mathcal{H}}_2 + \hat{\mathcal{H}}_{12} + \frac{\hbar^2 \hat{L}^2}{2\mu R^2} | a' \rangle. \quad (11)$$

The coupled equations (10) are solved by propagating a complete set of independent solution vectors from  $R_{\text{min}}$ , deep in the inner classically forbidden region, to  $R_{\text{max}}$ , large enough that the effects of the interaction potential have died off.

### C. Basis sets and matrix elements

The basis functions may be written  $|a\rangle \equiv |\alpha_1\rangle|\alpha_2\rangle|LM_L\rangle$ , where  $|\alpha_1\rangle$  and  $|\alpha_2\rangle$  are basis functions for atoms A and B, and  $M_X$  (or  $m_X$ ) denotes the projection of the angular momentum  $X$  along the axis of the magnetic field. We use two different basis sets, with common  $|\alpha_1\rangle = |i_1 m_{i1}\rangle |s_1 m_{s1}\rangle$ . The difference occurs in the description of atom B, for which we used both a totally uncoupled basis set  $|i_2 m_{i2}\rangle |l_2 m_{l2}\rangle |s_2 m_{s2}\rangle$  and an ‘*ls*-coupled’ basis set  $|i_2 m_{i2}\rangle |(l_2 s_2) j_2 m_{j2}\rangle$ . We have verified that scattering calculations in these two basis sets give identical results.

In a static magnetic field, the only conserved quantities are the projection  $M_{\text{tot}}$  of the total angular momentum and the total parity  $P$  of the system, which are explicitly  $M_{\text{tot}} = m_{i1} + m_{s1} + m_{i2} + m_{l2} + m_{s2} + M_L = m_{i1} + m_{s1} + m_{i2} + m_{j2} + M_L$  and  $P = p_1 p_2 (-1)^L$ , where  $p_1$  and  $p_2$  are the parities of atoms A and B. The coupled equations

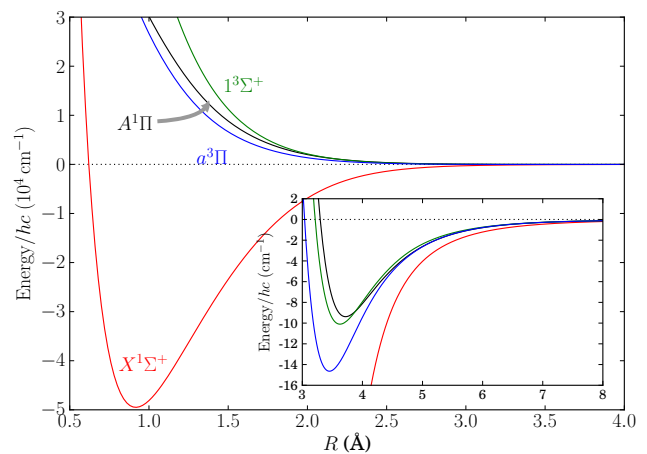


FIG. 1. (Color online) Ground ( $X^1\Sigma^+$ ) and excited ( $A^1\Pi$ ,  $1^3\Sigma^+$ ,  $a^3\Pi$ ) electronic states of H+F. The inset shows the relatively shallow Van der Waals wells for the excited states.

are therefore constructed and solved separately for each combination of  $M_{\text{tot}}$  and  $P$ .

Constructing the coupled equations (10) requires evaluating the matrix elements of all the terms in  $\hat{\mathcal{H}}_1$ ,  $\hat{\mathcal{H}}_2$  and  $\hat{\mathcal{H}}_{12}$  in the chosen basis set. The resulting matrix elements are given in Appendix A. The parameters for  $^{19}\text{F}$  hyperfine Hamiltonian were taken from Ref. [31].

### D. Interaction potentials

The interaction between the  $\text{H}(^2\text{S}_{1/2})$  and  $\text{F}(^2\text{P})$  atoms gives rise to four electronic states, shown in Fig. 1. The  $X^1\Sigma^+$  state is strongly chemically bound, with a well about  $50,000 \text{ cm}^{-1}$  (over 6 eV) deep near  $R = 0.9 \text{ Å}$ . By contrast, the  $A^1\Pi$ ,  $1^3\Sigma^+$  and  $a^3\Pi$  excited states are weakly bound, with long-range Van der Waals wells between 8 and  $15 \text{ cm}^{-1}$  deep at about  $3.5 \text{ Å}$ .

The potential curve for the ground state of HF has been determined very accurately by Coxon and Hajigeorgiou [38] from a global least-squares fit of all the spectroscopic data available in the literature. However, this curve is not strictly the curve for the pure  $^1\Sigma^+$  state: close to dissociation, it should be interpreted as the lowest eigenvalue of a fixed- $R$  electronic Hamiltonian, including spin-orbit coupling, which correlates with the  $^2\text{P}_{3/2}$  ground state of F. We have therefore used curves for the three excited states obtained by Brown and Balint-Kurti [39] from multi-reference configuration interaction (MRCI) calculations, and determined the  $^1\Sigma^+$  potential so that the lowest eigenvalue of the  $\Omega = 0$  matrix [40]

$$\begin{pmatrix} V_1^{\text{diab}} - \frac{1}{2}a_{\text{so}} & \frac{1}{\sqrt{2}}a_{\text{so}} \\ \frac{1}{\sqrt{2}}a_{\text{so}} & V_2^{\text{diab}} \end{pmatrix}, \quad (12)$$

matches the ground-state curve of Coxon and Hajigeorgiou [38]. Here,  $1 \equiv ^3\Pi_{0,e}$  and  $2 \equiv ^1\Sigma_{0,e}$  as seen in Fig. 1.

In this calculation, we neglected the  $R$ -dependence of the spin-orbit Hamiltonian. The resulting points for all 4 curves were inter-/extrapolated using the reproducing kernel Hilbert space (RKHS) method [41–43], with the  $C_6$ ,  $C_8$  and  $C_{10}$  dispersion coefficients constrained to match the scaled values of Ref. [44].

### E. Numerical methods

The coupled equations (10) are constructed in the primitive basis sets described in section II C. The basis set includes partial waves up to  $L_{\max} = 8$ , which is well converged. There are typically 100 to 200 channels, depending on  $M_{\text{tot}}$  and parity.

The coupled equations are solved using the hybrid log-derivative Airy method of Alexander and Manolopoulos [45], using a fixed-step-size log-derivative propagator for  $0.5 \leq R \leq 25$  Å, with  $\Delta R = 0.005$  Å, and a variable-step-size Airy propagator for  $25 \leq R \leq 10,000$  Å. The wavefunction log-derivative matrix is transformed at  $R_{\max} = 10,000$  Å into a basis set in which  $\mathcal{H}_1$ ,  $\mathcal{H}_2$  and  $\hat{L}^2$  are diagonal [28], and the transformed channel functions are matched to the standard scattering boundary conditions [46]. This gives the S-matrix from which the state-to-state cross sections and scattering lengths are calculated.

## III. RESULTS AND DISCUSSION

### A. Atomic hyperfine and Zeeman levels

Figure 2(a) shows the energy levels of the H atom in a magnetic field. For sympathetic cooling, we consider collisions with atoms that are magnetically trapped in the doubly-polarized state  $|^2S_{1/2}, m_{sH} = +\frac{1}{2}, m_{iH} = +\frac{1}{2}\rangle$ , designated  $H_d$  and shown as a solid blue line in Fig. 2(a).

Fig. 2(b) shows the corresponding energy levels of the  $^{19}\text{F}$  atom. We have carried out calculations on H+F collisions for the two low-field-seeking initial states shown as solid blue lines. These correspond to  $|^2P_{3/2}, f_F = 1, m_{fF} = +1\rangle$  and  $|^2P_{3/2}, f_F = 2, m_{fF} = +2\rangle$ , and are designated  $F_c$  and  $F_h$  respectively.

Hydrogen atoms cannot yet be laser-cooled, because the laser required to drive the  $2^2P \leftarrow 1^2S$  transition (Lyman- $\alpha$ ) is not available. Nevertheless, magnetically trapped hydrogen atoms in the state  $H_d$  have been produced at temperatures of 40 to 100 mK and densities up to  $3 \times 10^{14} \text{ cm}^{-3}$  by purely cryogenic methods [47, 48], and then evaporatively cooled to produce a Bose-Einstein condensate (BEC) of  $10^9$  atoms at a temperature around 50  $\mu\text{K}$  and densities between  $10^{14}$  and  $5 \times 10^{15} \text{ cm}^{-3}$  [49]. In addition, Zeeman deceleration and magnetic trapping of hydrogen has recently been demonstrated [50–53], although at higher temperatures and lower number densities. For sympathetic cooling purposes BEC is unneces-

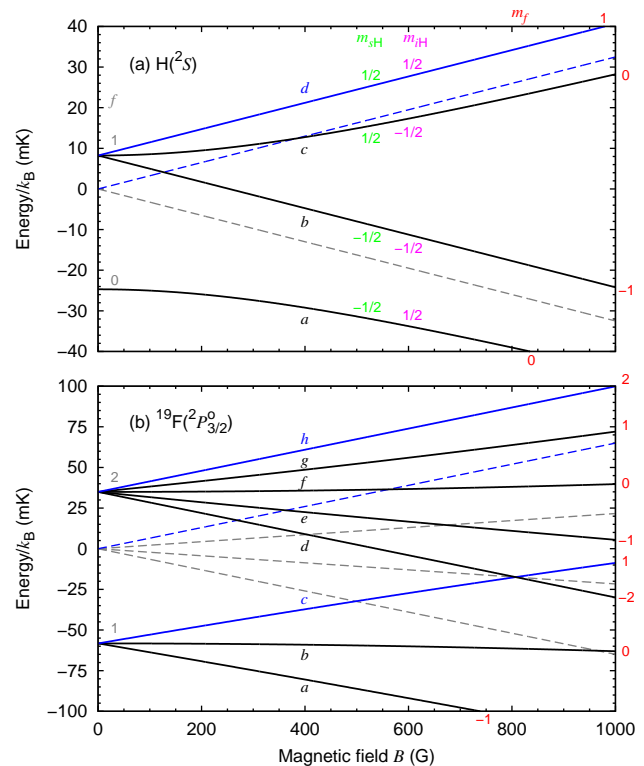


FIG. 2. (Color online) Magnetic-field dependence of the energy levels for: (a)  $\text{H}(^2S)$  and (b)  $^{19}\text{F}(^2P_{3/2}^o)$ . Solid (dashed) lines correspond to the inclusion (exclusion) of hyperfine terms. Scattering calculations were carried out for the magnetically trappable states highlighted in blue.

sary, but the large densities and cloud sizes achievable by cryogenic methods are very valuable.

### B. Elastic and inelastic collisions

Figure 3(a) shows the elastic and total inelastic cross sections as a function of collision energy for collisions between hydrogen atoms in state  $H_d$  and fluorine atoms in state  $F_h$ . These collisions are spin-stretched, meaning that both atoms have their maximum values of all projection quantum numbers. Because of this, collisions that change a projection quantum number on either atom must necessarily change  $M_L$ , and this means that s-wave collisions (incoming  $L = 0$ ) must have outgoing  $L \geq 2$  [54, 55]. s-wave inelastic collisions are therefore suppressed by an  $L = 2$  centrifugal barrier in the outgoing channel, which for H+F collisions is 3.2 K high. For p-wave collisions, with incoming  $L = 1$ , the barrier is lower (614 mK), but in this case there is a barrier in both the incoming and outgoing channels. Figure 3(a) shows that the elastic cross section is dominated by s-wave collisions at energies up to about 400 mK. p-wave contributions to inelastic cross sections are significant above about 1 mK and d-wave collisions contribute significantly above about 3 K. The low-energy inelastic cross sections are larger at

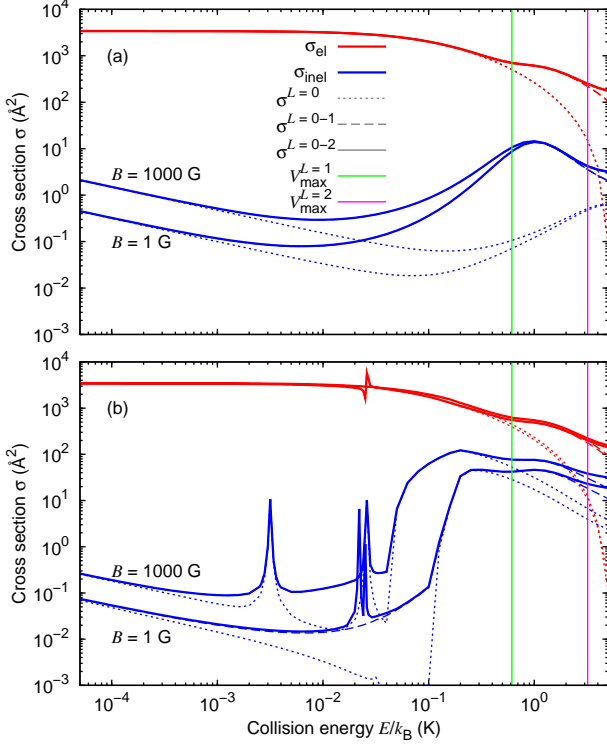


FIG. 3. (Color online) Elastic and total inelastic cross sections as a function of collision energy, for  $B = 1$  and 1000 G. Results are shown for collisions of spin-stretched H ( $H_d$ ) with: (a) spin-stretched F ( $F_h$ ), and (b)  $F_c$  (the initial states highlighted in Fig. 2). Solid lines include s-, p- and d-wave contributions, dashed lines include s-, p-wave contributions and dotted lines are the s-wave cross sections. The vertical lines show the heights of the p and d-wave centrifugal barriers.

1000 G than at 1 G because the kinetic energy release for inelastic collisions increases with field and helps to overcome the centrifugal barrier in the outgoing channel. Nevertheless, the ratio of elastic to inelastic cross sections remains above 100 for both fields at energies up to 5 K, except in the region of a p-wave shape resonance in the incoming channel around 1 K.

Figure 4(a) shows state-to-state cross sections for the most important product channels in  $H_d + F_h$  collisions, which help to understand the collision mechanisms. For spin-stretched collisions, the dominant channels are those in which the F state changes and the H atom is a spectator. This suggests that the dominant coupling is the anisotropy of the triplet potentials  $V_2^1(R)$  (Eq. (7)), combined with the spin-orbit coupling. This term can change  $m_{F_F}$  by up to 2, and formation of  $F_b$  and  $F_c$  is preferred over formation of  $F_f$  and  $F_g$  because the larger kinetic energy release for the former pair helps reduce centrifugal suppression.

Figure 3(b) shows elastic and total inelastic cross sections for  $H_d + F_c$  collisions, with the F atom initially in a magnetically trappable state that correlates with  $f_F = 1$ ; this state is *not* spin-stretched and has  $m_{F_F} = +1$ . At

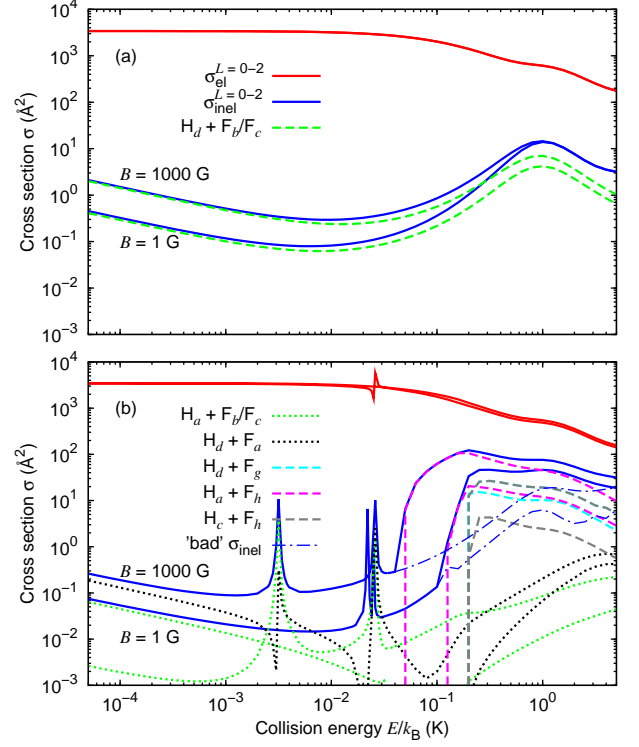


FIG. 4. (Color online) The most important state-to-state cross sections as a function of collision energy, for  $B = 1$  and 1000 G. Results are shown for collisions of spin-stretched H ( $H_d$ ) with: (a) spin-stretched F ( $F_h$ ), and (b)  $F_c$ . The line for  $H_d + F_g$  is hidden underneath that for  $H_c + F_h$  in the steep region near their thresholds.

1000 G the dominant channels at low collision energy are those in which the state of the H atom does not change, as shown in Fig. 4(b). The inelastic cross sections are actually *smaller* than for spin-stretched collisions at low energy, because the kinetic energy releases are lower and there is more centrifugal suppression. At 1 G the centrifugal suppression is so strong that a different mechanism takes over: the weak dipolar interaction can drive long-range inelastic collisions that take place *outside* the centrifugal barrier [56, 57], producing  $H_a$  and  $F_b$  or  $F_c$ ; Fig. 4(b) shows that this is the dominant low-energy mechanism at 1 G.

There are also narrow resonances for  $H_d + F_c$  collisions, between 20 and 30 mK at 1 G and around 3 and 30 mK at 1000 G, which produce peaks in the inelastic cross sections. These are due to resonances in the singlet states and their positions are very sensitive to changes in the singlet potentials. However, they are narrow enough to have little effect on sympathetic cooling.

At higher energies, additional inelastic channels open. Collisions to form  $H_a + F_h$  are possible at collision energies above 60 mK at 1 G and above 24 mK at 1000 G. There are also channels forming  $H_c + F_h$  and  $H_d + F_g$  that open near 100 mK for both fields. All these collisions

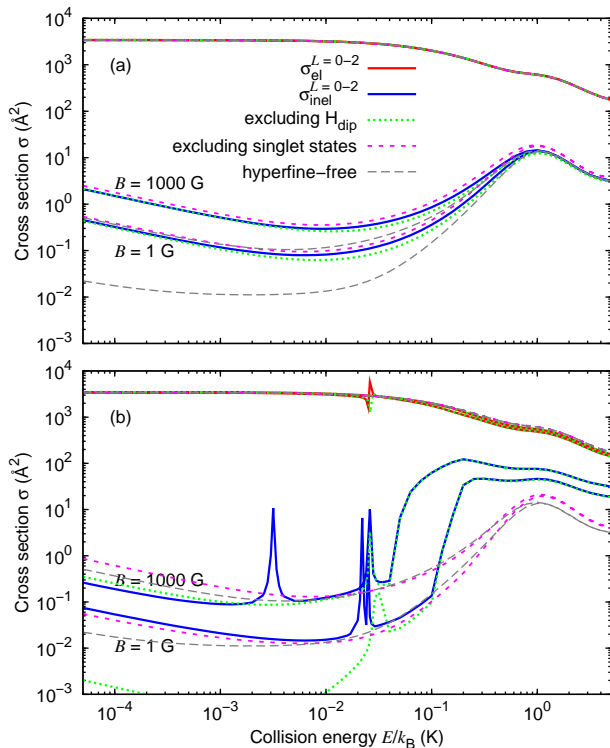


FIG. 5. (Color online) Elastic and total inelastic cross sections as a function of collision energy, for  $B = 1$  and 1000 G, from both full coupled-channel calculations and a variety of approximations. Results are shown for collisions of spin-stretched H ( $H_d$ ) with: (a) spin-stretched F ( $F_h$ ), and (b)  $F_c$ .

conserve  $m_{fF} + m_{fH}$ , so are not centrifugally suppressed and dominate the inelasticity above their threshold energies. They are driven by the *difference* between the singlet and triplet potentials, and we refer to them as “spin-exchange” collisions by analogy with the corresponding process in collisions between alkali-metal atoms. These collisions and their consequences will be considered in more detail below. However, we will note here that they do *not* lead to trap loss for F atoms, and will not necessarily prevent sympathetic cooling; the dot-dashed lines in Fig. 4(b) show the inelastic cross sections obtained if the spin-exchange collisions are excluded.

Figure 5 shows the results for  $H_d + F_h$  and  $H_d + F_c$  collisions with various approximations. First, the green dotted lines show the results of excluding the dipolar interaction  $\mathcal{H}_{\text{dip}}$  between the atoms; it may be seen that this is a good approximation for spin-stretched collisions, and also for non-spin-stretched collisions at 1000 G, where the kinetic energy release is substantial and collisions that change only  $m_{fF}$  dominate (driven by the potential anisotropy, and subject to centrifugal suppression). However, it dramatically underestimates the low-energy inelastic cross sections at 1 G, which are driven by the dipolar interaction as discussed above.

The long dashed grey lines in Fig. 5 show the effect

of neglecting hyperfine interactions (which produces the same state for  $F_h$  and  $F_c$ , with  $m_{jF} = +3/2$ , so the hyperfine-free lines are the same in both panels). This approximation significantly reduces the inelastic cross sections: the difference arises from the additional kinetic energy released in the presence of hyperfine interactions. This effect is similar to the one that we have identified and discussed in Mg+NH collisions [23].

Lastly, the short dashed purple lines in Fig. 5 show the effect of setting the singlet potentials equal to the corresponding triplet potentials. This approximation is not necessary for H+F collisions, but for atom+molecule collisions such as H+NH and H+OH [20] it is difficult or impossible to converge scattering calculations in which the deep low-spin surfaces (corresponding to  $H_2O$  or  $NH_2$ ) are included with their full depth. H+F allows this approximation to be tested. It may be seen that including the full singlet curves has only a fairly small effect (20 to 30%) for spin-stretched collisions; this is expected, because pairs of spin-stretched atoms or molecules interact entirely on the highest-spin surface, and lower-spin surfaces can contribute only after one of the spin projections has changed. For the non-spin-stretched collisions shown in Fig. 5(b), the effect is small at 1 G, except near the narrow singlet resonances, but considerably larger (up to a factor of 6) at 1000 G below 40 mK. In addition, neglecting the difference between the singlet and triplet curves prevents the spin-exchange excitation collisions that become important at higher collision energies.

### C. Sympathetic cooling

Using a hard-sphere model, deCarvalho *et al.* [26] found that the temperatures difference between the warm and coolant species after  $k$  collisions is given by

$$\frac{T_2^k - T_1}{T_2^0 - T_1} = \exp\left(-\frac{k}{\kappa}\right), \quad (13)$$

where the number of collisions  $\kappa$  required to reduce the temperature difference by a factor of  $e$  is

$$\kappa = \frac{(m_1 + m_2)^2}{2m_1m_2} = \frac{1}{2} \left(1 + \frac{m_1}{m_2}\right) \left(1 + \frac{m_2}{m_1}\right) \quad (14)$$

and thus depends solely on the mass ratio. In our case,  $\kappa \approx 10.5$ .

Figure 6(a) shows the ratio  $\gamma$  of elastic to inelastic cross sections, as a function of collision energy and magnetic field, for  $^{19}\text{F}$  initially in state  $F_h$ . The diagonal black line shows the field at which the Zeeman energy is  $6k_B T$ , so that 99.9% of F atoms at temperature  $T$  sample fields below the line. It may be seen that  $\gamma$  exceeds 1,000, and sympathetic cooling of  $^{19}\text{F}$  atoms is thus predicted to be successful, for almost all fields and energies up to 5 K. The ratio reduces to around 40 near 1 K, due to the p-wave shape resonance discussed above, but this should not prevent overall cooling.



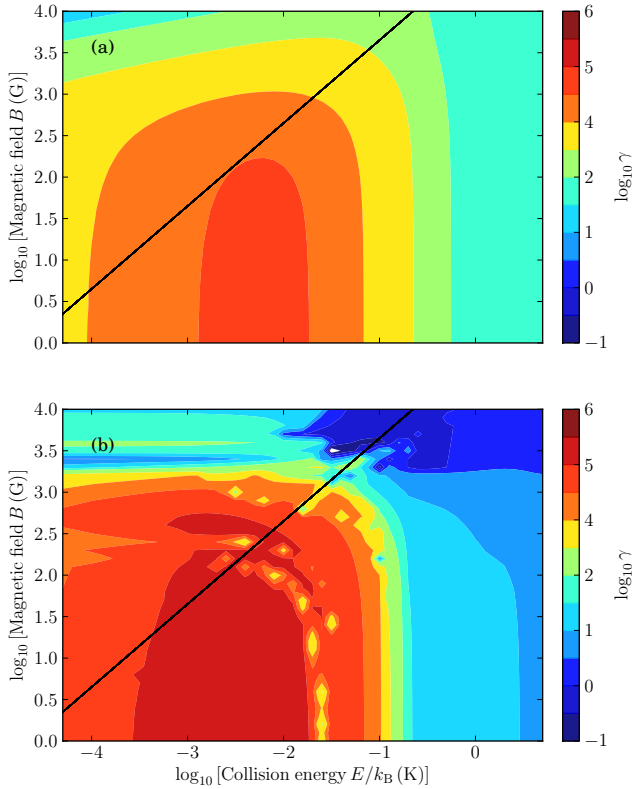


FIG. 6. (Color online) Contour plots of the ratio  $\gamma$  of elastic to total inelastic cross sections as a function of collision energy and magnetic field. Results are shown for collisions of spin-stretched H ( $H_d$ ) with: (a) spin-stretched F ( $F_h$ ), and (b)  $F_c$  (the initial states highlighted in Fig. 2). The apparently uneven behavior of the contours in (b) arises because our grid cannot fully capture the sharp singlet resonances, which on a finer grid would appear as very narrow bands rather than isolated peaks.

For F atoms initially in state  $F_c$ , the situation is rather more complicated. Figure 6(b) shows the ratio  $\gamma$  for this state. At energies and fields below about 50 mK,  $\gamma$  for  $F_c$  is actually more favorable than for  $F_h$ . However, at higher energies the spin-exchange collisions described above can occur, exciting the F atom to  $F_h$  and transferring the H atom to  $H_a$ . The latter is an untrapped state, so H atoms in the  $H_a$  state will be removed from the trap and will not be available for the reverse process. However, the F atoms transferred to state  $F_h$  will have *lost* kinetic energy, so will remain trapped. If F atoms in the  $F_c$  state start at a temperature of (say) 500 mK, it will require about 25 elastic collisions to cool them to 50 mK (or somewhat more if the H atom temperature is significant). However, the cross section for spin-exchange collisions is about 1/10 of that for elastic collisions, so almost all the atoms will be in state  $F_h$  by the time they have cooled to 50 mK. Sympathetic cooling will then proceed mostly in state  $F_h$  even if the atoms were initially in state  $F_c$ .

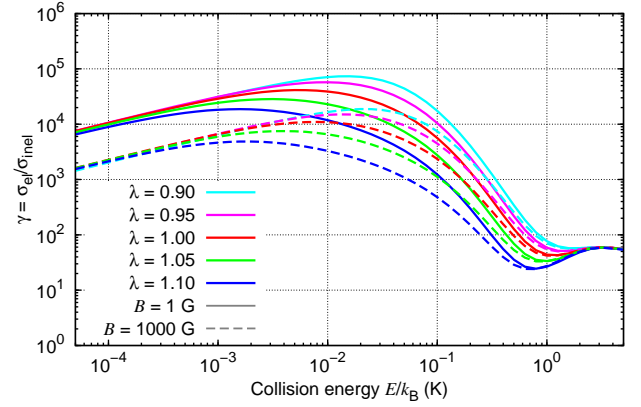


FIG. 7. (Color online) Variation of the ratio  $\gamma$  of elastic to total inelastic cross sections for spin-stretched collisions ( $H_d + F_h$ ) at 1 G (solid curves) and 1000 G (dashed curves), as a function of a scaling factor  $\lambda$  applied to the excited-state potential curves.

#### D. Sensitivity to the interaction potential

The ground-state potential for HF is very well known from spectroscopic experiments [38], and as seen above has relatively little effect on the inelastic cross sections, particularly for atoms in spin-stretched states. However, there is some uncertainty in the potential curves for the three excited states. To explore the effect of this uncertainty on the cross sections, we have carried out calculations on sets of potentials obtained by scaling the three excited curves by common factors of  $\lambda = 0.90, 0.95, 1.05$  and  $1.10$ . This slightly changes the  $^1\Sigma^+$  curve as well. The resulting values of the ratio  $\gamma$  for spin-stretched collisions at 1 G and 1000 G are shown in Fig. 7. It may be seen that  $\gamma$  is almost independent of  $\lambda$  below 1 mK, but that the differences increase at higher energies. The main effect is that, as  $\lambda$  is increased, the p-wave resonance near 1 K drops to slightly lower energies and become higher and narrower. As seen in section III C, the key quantity is the energy at which the ratio  $\gamma$  drops below 100: the worst case is for  $\lambda = 1.10$  at 1000 G, where this is reduced from around 500 mK to around 250 mK. We conclude that plausible variations in the potential may slightly affect the temperature at which sympathetic cooling starts to work, but do not alter the qualitative conclusions.

The  $^1\Sigma^+$ ,  $^1\Pi$ ,  $^3\Sigma^+$  and  $^3\Pi$  potential curves used in the present work have scattering lengths of  $-16.3$ ,  $-107$ ,  $-284$  and  $12.1$  Å, respectively. These may be compared with the mean scattering length  $\bar{a}$  [58], which for this system is  $3.2$  Å. The isotropic triplet potential  $\hat{V}_0^1(R)$  supports one s-wave bound state just below threshold. As  $\lambda$  is reduced from 1, this state comes closer to threshold; the s-wave elastic and inelastic cross sections both increase, but by similar factors, so that  $\gamma$  is almost unchanged at low energy. It would require an implausibly small value  $\lambda \approx 0.8$  to bring this state all the way up to

threshold.

#### IV. CONCLUSIONS

Ultracold hydrogen atoms are a very promising coolant for atoms and molecules that are not amenable to laser Doppler cooling. In previous work [20], we have shown that sympathetic cooling with atomic hydrogen is likely to work for molecules such as NH and OH, from starting temperatures of 100-1000 mK down to the microkelvin regime. In the present paper we have shown that this is also true for atomic fluorine, from starting temperatures of 500 to 1000 mK. Other halogen atoms are likely to behave similarly, although more collisions are needed for thermalization because of the high mass ratio.

The calculations on F+H collisions have also allowed us to test approximations made for the molecular systems. In particular, for F+H it was possible to include the deep singlet ground state fully in the calculations. Despite its depth, the singlet state was found to have little effect on collisions involving spin-stretched states. This gives us confidence that approximating the deep low-spin surfaces, as was necessary for NH+H and OH+H [20], is a good approximation.

#### ACKNOWLEDGMENTS

The authors are grateful to Dermot Green and Ruth Le Sueur for valuable discussions and to EPSRC for funding.

- 
- [1] M. H. Anderson, J. R. Ensher, M. R. Matthews, C. E. Wieman, and E. A. Cornell, *Science* **269**, 198 (1995).
  - [2] C. C. Bradley, C. A. Sackett, J. J. Tollett, and R. G. Hulet, *Phys. Rev. Lett.* **75**, 1687 (1995).
  - [3] K. B. Davis, M. O. Mewes, M. R. Andrews, N. J. van Druten, D. S. Durfee, D. M. Kurn, and W. Ketterle, *Phys. Rev. Lett.* **75**, 3969 (1995).
  - [4] B. DeMarco and D. S. Jin, *Science* **285**, 1703 (1999).
  - [5] A. G. Truscott, K. E. Strecker, W. I. McAlexander, G. B. Partridge, and R. G. Hulet, *Science* **291**, 2570 (2001).
  - [6] M. R. Andrews, C. G. Townsend, H.-J. Miesner, D. S. Durfee, D. M. Kurn, and W. Ketterle, *Science* **275**, 637 (1997).
  - [7] M. R. Matthews, B. P. Anderson, P. C. Haljan, D. S. Hall, C. E. Wieman, and E. A. Cornell, *Phys. Rev. Lett.* **83**, 2498 (1999), URL <http://link.aps.org/doi/10.1103/PhysRevLett.83.2498>.
  - [8] S. Burger, K. Bongs, S. Dettmer, W. Ertmer, K. Sengstock, A. Sanpera, G. V. Shlyapnikov, and M. Lewenstein, *Phys. Rev. Lett.* **83**, 5198 (1999), URL <http://link.aps.org/doi/10.1103/PhysRevLett.83.5198>.
  - [9] J. Denschlag, J. E. Simsarian, D. L. Feder, C. W. Clark, L. A. Collins, J. Cubizolles, L. Deng, E. W. Hagley, K. Helmerson, W. P. Reinhardt, et al., *Science* **287**, 97 (2000).
  - [10] I. Bloch, *Nature Phys.* **1**, 23 (2005).
  - [11] O. Dulieu and C. Gabbanini, *Rep. Prog. Phys.* **72**, 086401 (2009).
  - [12] L. D. Carr, D. DeMille, R. V. Krems, and J. Ye, *New J. Phys.* **11**, 055049 (2009).
  - [13] R. V. Krems, B. Friedrich, and W. C. Stwalley, eds., *Cold Molecules: Theory, Experiment, Applications* (Taylor & Francis, London, 2009), ISBN 978-1-4200-5903-8.
  - [14] C. Chin, R. Grimm, P. Julienne, and E. Tiesinga, *Rev. Mod. Phys.* **82**, 1225 (2010).
  - [15] P. F. Weck and N. Balakrishnan, *Int. Rev. Phys. Chem.* **25**, 283 (2006).
  - [16] D. Herschbach, *Faraday Discuss.* **142**, 9 (2009).
  - [17] W. G. Doherty, M. T. Bell, T. P. Softley, A. Rowland, E. Wrede, and D. Carty, *Phys. Chem. Chem. Phys.* **13**, 8441 (2011), URL <http://dx.doi.org/10.1039/C0CP02472D>.
  - [18] A. Trottier, E. Wrede, and D. Carty, *Mol. Phys.* **109**, 725 (2011).
  - [19] E. Narevicius, C. G. Parthey, A. Libson, M. F. Riedel, U. Even, and M. G. Raizen, *New J. Phys.* **9**, 96 (2007).
  - [20] M. L. González-Martínez and J. M. Hutson (2013), submitted for publication in *Physical Review Letters*; arXiv:1305.6282.
  - [21] A. O. G. Wallis and J. M. Hutson, *Phys. Rev. Lett.* **103**, 183201 (2009).
  - [22] A. O. G. Wallis, E. J. J. Longdon, P. S. Żuchowski, and J. M. Hutson, *Eur. Phys. J. D* **65**, 151 (2011).
  - [23] M. L. González-Martínez and J. M. Hutson, *Phys. Rev. A* **84**, 052706 (2011), URL <http://link.aps.org/doi/10.1103/PhysRevA.84.052706>.
  - [24] H. L. Bethlem, G. Berden, F. M. H. Crompvoets, R. T. Jongma, A. J. A. van Roij, and G. Meijer, *Nature* **406**, 491 (2000).
  - [25] J. D. Weinstein, R. deCarvalho, T. Guillet, B. Friedrich, and J. M. Doyle, *Nature* **395**, 148 (1998).
  - [26] R. deCarvalho, J. M. Doyle, B. Friedrich, T. Guillet, J. Kim, D. Patterson, and J. D. Weinstein, *Eur. Phys. J. D* **7**, 289 (1999).
  - [27] J. M. Hutson and S. Green, *computer code MOLSCAT, version 14*, CCP6, Daresbury (1994).
  - [28] M. L. González-Martínez and J. M. Hutson, *Phys. Rev. A* **75**, 022702 (2007), URL <http://link.aps.org/doi/10.1103/PhysRevA.75.022702>.
  - [29] E. U. Condon and G. H. Shortley, *The Theory of Atomic Spectra* (Cambridge University Press, Cambridge, 1970), ISBN 0-521-09209-4.
  - [30] R. E. Trees, *Phys. Rev.* **92**, 308 (1953).
  - [31] J. S. M. Harvey, *Proc. R. Soc. Lond. A* **285**, 581 (1965).
  - [32] Note1, the effect of nuclear shielding factors is extremely small and has been neglected in the present work.
  - [33] J. M. Brown and A. Carrington, *Rotational Spectroscopy of Diatomic Molecules* (Cambridge University Press, Cambridge, 2003), p. 351.
  - [34] R. V. Krems, G. C. Groenenboom, and A. Dalgarno, *J. Phys. Chem. A* **108**, 8941 (2004).
  - [35] J. M. Brown and A. Carrington, *Rotational Spectroscopy of Diatomic Molecules* (Cambridge University Press, Cambridge, 2003).



- [36] P. S. Żuchowski, J. Aldegunde, and J. M. Hutson, Phys. Rev. Lett. **105**, 153201 (2010).
- [37] D. A. Brue and J. M. Hutson, Phys. Rev. A **87**, 052709 (2013).
- [38] J. A. Coxon (2012), private communication.
- [39] A. Brown and G. G. Balint-Kurti, J. Chem. Phys. **113**, 1870 (2000).
- [40] M. Aubert-Frécon, G. Hadinger, S. Magnier, and S. Rousseau, J. Mol. Spectrosc. **188**, 182 (1998).
- [41] T.-S. Ho and H. Rabitz, J. Chem. Phys. **104**, 2584 (1996).
- [42] P. Soldán and J. M. Hutson, J. Chem. Phys. **112**, 4415 (2000).
- [43] T.-S. Ho and H. Rabitz, J. Chem. Phys. **113**, 3960 (2000).
- [44] O. Zatsarinny, K. Bartschat, J. Mitroy, and J.-Y. Zhang, J. Chem. Phys. **130**, 124310 (2009).
- [45] M. H. Alexander and D. E. Manolopoulos, J. Chem. Phys. **86**, 2044 (1987).
- [46] B. R. Johnson, J. Comp. Phys. **13**, 445 (1973).
- [47] H. F. Hess, G. P. Kochanski, J. M. Doyle, N. Masuhara, D. Kleppner, and T. J. Greytak, Phys. Rev. Lett. **59**, 672 (1987), URL <http://link.aps.org/doi/10.1103/PhysRevLett.59.672>.
- [48] R. van Roijen, J. J. Berkhout, S. Jaakkola, and J. T. M. Walraven, Phys. Rev. Lett. **61**, 931 (1988), URL <http://link.aps.org/doi/10.1103/PhysRevLett.61.931>.
- [49] D. G. Fried, T. C. Killian, L. Willmann, D. Landhuis, S. C. Moss, D. Kleppner, and T. J. Greytak, Phys. Rev. Lett. **81**, 3811 (1998), URL <http://link.aps.org/doi/10.1103/PhysRevLett.81.3811>.
- [50] N. Vanhaecke, U. Meier, M. Andrist, B. H. Meier, and F. Merkt, Phys. Rev. A **75**, 031402(R) (2007).
- [51] S. D. Hogan, D. Sprecher, M. Andrist, N. Vanhaecke, and F. Merkt, Phys. Rev. A **76**, 023412 (2007).
- [52] S. D. Hogan, A. W. Wiederkehr, H. Schmutz, and F. Merkt, Phys. Rev. Lett. **101**, 143001 (2008).
- [53] S. D. Hogan, C. Seiler, and F. Merkt, Phys. Rev. Lett. **103**, 123001 (2009), URL <http://link.aps.org/doi/10.1103/PhysRevLett.103.123001>.
- [54] A. V. Avdeenkov and J. L. Bohn, Phys. Rev. A **64**, 052703 (2001).
- [55] A. Volpi and J. L. Bohn, Phys. Rev. A **65**, 052712 (2002).
- [56] L. M. C. Janssen, P. S. Żuchowski, A. van der Avoird, G. C. Groenenboom, and J. M. Hutson, Phys. Rev. A **83**, 022713 (2011).
- [57] L. M. C. Janssen, A. van der Avoird, and G. C. Groenenboom, Eur. Phys. J. D **65**, 177 (2011).
- [58] G. F. Gribakin and V. V. Flambaum, Phys. Rev. A **48**, 546 (1993).

## Appendix A: Matrix Elements

This Appendix describes the matrix elements used in the coupled-channel calculations in both the uncoupled and  $ls$ -coupled basis sets described in Section II C.

The matrix elements for  $\hat{L}^2$  are totally diagonal in both basis sets and are given by  $L(L+1)$ .

Several terms in our Hamiltonian (1) share the structure  $\hat{\mathcal{H}}_{j_1 j_2} = \kappa \hat{j}_1 \cdot \hat{j}_2$ , where  $\kappa$  is a scalar while  $\hat{j}_1$  and  $\hat{j}_2$  are vector operators. Their matrix elements in the basis set  $|j_1 m_{j_1}\rangle |j_2 m_{j_2}\rangle$ , are

$$\begin{aligned} \langle j_2 m_{j_2} | \langle j_1 m_{j_1} | \hat{\mathcal{H}}_{j_1 j_2} | j_1 m'_{j_1} \rangle | j_2 m'_{j_2} \rangle &= \delta_{m_{j_1} m'_{j_1}} \delta_{m_{j_2} m'_{j_2}} \kappa m_{j_1} m_{j_2} \\ &+ \delta_{m_{j_1} m'_{j_1} \pm 1} \delta_{m_{j_2} m'_{j_2} \mp 1} \frac{\kappa}{2} [j_1(j_1+1) - m_{j_1} m'_{j_1}]^{1/2} [j_2(j_2+1) - m_{j_2} m'_{j_2}]^{1/2}. \end{aligned} \quad (\text{A1})$$

Such terms can mix functions with adjacent values of the projections of  $\hat{j}_1$  and  $\hat{j}_2$ , but preserve the sum  $m_{12} = m_{j_1} + m_{j_2}$ . Here and throughout this appendix, the matrix elements are fully diagonal with respect to quantum numbers that do not explicitly appear in their definitions.

The matrix elements of  $\hat{\mathcal{H}}_1$  depend on  $|\alpha_1\rangle$  only and are thus identical in the two basis sets. Those for  $\hat{\mathcal{H}}_{F,1}$  are of the form (A1), while those of  $\hat{\mathcal{H}}_{Z,1}$  are totally diagonal and are given by

$$\langle s_1 m_{s1} | \langle i_1 m_{i1} | \hat{\mathcal{H}}_{Z,1} | i_1 m_{i1} \rangle | s_1 m_{s1} \rangle = (g_S \mu_B m_{s1} - g_I \mu_N m_{i1}) B. \quad (\text{A2})$$

The matrix elements of  $\hat{\mathcal{H}}_2$  depend on  $|\alpha_2\rangle$  only. Those for  $\hat{\mathcal{H}}_{so}$  are independent of the nuclear spin quantum numbers. They have the form (A1) in the uncoupled basis set, while in the  $ls$ -coupled basis set they are completely diagonal and are given by

$$\langle (l_2 s_2) j_2 m_{j_2} | \hat{\mathcal{H}}_{so} | (l_2 s_2) j_2 m_{j_2} \rangle = \frac{a_{so}}{2} [j_2(j_2+1) - l_2(l_2+1) - s_2(s_2+1)]. \quad (\text{A3})$$

The matrix elements for the dipolar component of  $\hat{\mathcal{H}}_{hf,2}$  are of the form (A1) in both basis sets (once  $\hat{j}_2$  is split into  $\hat{l}_2 + \hat{s}_2$  for evaluation in the uncoupled basis set).

The matrix elements for the quadrupolar term are readily calculated by first rearranging

$$\langle \alpha_2 | \hat{\mathcal{H}}_Q | \alpha'_2 \rangle = 2b_j \left( 2 \sum_{\alpha''_2} \langle \alpha_2 | \hat{i}_2 \cdot \hat{j}_2 | \alpha''_2 \rangle \langle \alpha''_2 | \hat{i}_2 \cdot \hat{j}_2 | \alpha'_2 \rangle + \langle \alpha_2 | \hat{i}_2 \cdot \hat{j}_2 | \alpha'_2 \rangle \right) \quad (\text{A4})$$

and then applying Eq. (A1) to each term. For instance, in the  $ls$ -coupled basis set

$$\begin{aligned} \langle i_2 m_{i2} | \langle (l_2 s_2) j_2 m_{j2} | \hat{\mathcal{H}}_Q | (l_2 s_2) j_2 m'_{j2} \rangle | i_2 m'_{i2} \rangle &= 2b_j \left\{ \delta_{m_{i2} m'_{i2}} \delta_{m_{j2} m'_{j2}} 3m_{i2} m_{j2} \right. \\ &+ \delta_{m_{i2} m'_{i2} \pm 1} \delta_{m_{j2} m'_{j2} \mp 1} \frac{1}{2} (2m_{i2} m_{j2} + 2m'_{i2} m'_{j2} + 1) [i_2(i_2 + 1) - m_{i2} m'_{i2}]^{1/2} [j_2(j_2 + 1) - m_{j2} m'_{j2}]^{1/2} \\ &+ \frac{1}{2} \sum_{m''_{i2} m''_{j2}} \delta_{m_{i2} m''_{i2} \pm 1} \delta_{m_{j2} m''_{j2} \mp 1} [i_2(i_2 + 1) - m_{i2} m''_{i2}]^{1/2} [j_2(j_2 + 1) - m_{j2} m''_{j2}]^{1/2} \\ &\left. \times \delta_{m''_{i2} m'_{i2} \pm 1} \delta_{m''_{j2} m'_{j2} \mp 1} [i_2(i_2 + 1) - m''_{i2} m'_{i2}]^{1/2} [j_2(j_2 + 1) - m''_{j2} m'_{j2}]^{1/2} \right\}, \end{aligned} \quad (\text{A5})$$

which is non-zero for  $\Delta m_{i2} = 0, \pm 1, \pm 2$  and  $\Delta m_{j2} = -\Delta m_{i2}$ , thus preserving the sum  $m_{i2} + m_{j2}$ . The uncoupled matrix elements are evaluated similarly by first splitting  $\hat{j}_2$  into  $\hat{l}_2 + \hat{s}_2$ .

The matrix elements for  $\hat{\mathcal{H}}_{Z,2}$  are totally diagonal in the uncoupled basis set,

$$\langle s_2 m_{s2} | \langle l_2 m_{l2} | \langle i_2 m_{i2} | \hat{\mathcal{H}}_{Z,2} | i_2 m_{i2} \rangle | l_2 m_{l2} \rangle | s_2 m_{s2} \rangle = (g'_L \mu_B m_{l2} + g_S \mu_B m_{s2} - g_{i2} \mu_N m_{i2}) B, \quad (\text{A6})$$

while in the  $ls$ -coupled basis set they are given by

$$\begin{aligned} &\langle (l_2 s_2) j_2 m_{j2} | \langle i_2 m_{i2} | \hat{\mathcal{H}}_{Z,2} | i_2 m_{i2} \rangle | (l_2 s_2) j'_2 m_{j2} \rangle \\ &= \left[ g_S \mu_B (-1)^{2j_2 + l_2 + s_2 - m_{j2} + 1} [s_2(s_2 + 1)(2s_2 + 1)(2j_2 + 1)(2j'_2 + 1)]^{1/2} \begin{pmatrix} j_2 & 1 & j'_2 \\ -m_{j2} & 0 & m_{j2} \end{pmatrix} \begin{Bmatrix} s_2 & j'_2 & l_2 \\ j_2 & s_2 & 1 \end{Bmatrix} \right. \\ &\quad + g'_L \mu_B (-1)^{j_2 + j'_2 + l_2 + s_2 - m_{j2} + 1} [l_2(l_2 + 1)(2l_2 + 1)(2j_2 + 1)(2j'_2 + 1)]^{1/2} \begin{pmatrix} j_2 & 1 & j'_2 \\ -m_{j2} & 0 & m_{j2} \end{pmatrix} \begin{Bmatrix} l_2 & j'_2 & s_2 \\ j_2 & l_2 & 1 \end{Bmatrix} \\ &\quad \left. - g_{i2} \mu_N m_{i2} \right] B, \end{aligned} \quad (\text{A7})$$

where  $(:::)$  and  $\{\{\cdot\cdot\cdot\}\}$  represent Wigner 3- $j$  and 6- $j$  symbols.  $\hat{\mathcal{H}}_{Z,2}$  can thus mix states with different  $j_2$  while preserving the projection  $m_{j2}$ : for fluorine, it couples the  $j_2 = 3/2$  and  $1/2$  states only for  $m_{j2} = -1/2$  or  $1/2$ .

The matrix elements of the electronic interaction potential in the uncoupled basis set are

$$\begin{aligned} &\langle LM_L | \langle s_2 m_{s2} | \langle l_2 m_{l2} | \langle s_1 m_{s1} | \hat{V} | s_1 m'_{s1} \rangle | l_2 m'_{l2} \rangle | s_2 m'_{s2} \rangle | L' M'_L \rangle \\ &= (-1)^{2(s_1 - s_2 + M_S) - m_{l2} + M'_L} (2l_2 + 1) [(2L + 1)(2L' + 1)]^{1/2} \sum_S (2S + 1) \begin{pmatrix} s_1 & s_2 & S \\ m_{s1} & m_{s2} & -M_S \end{pmatrix} \begin{pmatrix} s_1 & s_2 & S \\ m'_{s1} & m'_{s2} & -M_S \end{pmatrix} \\ &\quad \times \sum_k \hat{V}_k^S(R) \begin{pmatrix} l_2 & k & l_2 \\ 0 & 0 & 0 \end{pmatrix} \begin{pmatrix} l_2 & k & l_2 \\ -m_{l2} & m_k & m'_{l2} \end{pmatrix} \begin{pmatrix} L & k & L' \\ 0 & 0 & 0 \end{pmatrix} \begin{pmatrix} L & k & L' \\ -M_L & -m_k & M'_L \end{pmatrix}, \end{aligned} \quad (\text{A8})$$

with  $M_S \equiv m_{s1} + m_{s2} = m'_{s1} + m'_{s2}$  and  $m_k \equiv M'_L - M_L$ . The matrix elements for the isotropic terms  $V_0^S$  are off-diagonal only in the  $m_s$  quantum numbers while preserving  $M_S$ . If  $l_2 = 0$ , these are the only couplings induced by  $\hat{V}$  and have been studied in detail in collisions of alkali atoms. For  $l_2 \neq 0$ , the anisotropic terms  $V_k^S$  ( $k \neq 0$ ) can additionally mix different partial waves and change  $m_{l2}$  independently of  $m_{s2}$ , thus changing their sum  $m_{j2}$  (such couplings exist even if  $s_1 = 0$ ).

The mixing of the electronic degrees of freedom makes it difficult to find an expression for the matrix elements of the electronic interaction in the  $ls$ -coupled basis set that has a simple physical interpretation. It is more convenient to evaluate these by transforming the matrix elements in the uncoupled representation (A8) using the standard vector-coupling formula,

$$|(l_2 s_2) j_2 m_{j2} \rangle = \sum_{m_{l2} m_{s2}} \langle l_2 m_{l2} s_2 m_{s2} | (l_2 s_2) j_2 m_{j2} \rangle | l_2 m_{l2} \rangle | s_2 m_{s2} \rangle. \quad (\text{A9})$$

If the extremely small nuclear contributions to the magnetic moments in  $\hat{\mathcal{H}}_{\text{dip}}$  are neglected, the matrix elements of  $\hat{\mathcal{H}}_{12}$  become diagonal in the nuclear projection quantum numbers. The matrix elements of the dipolar interaction

in the uncoupled basis set are given by

$$\begin{aligned}
& \langle LM_L | \langle s_2 m_{s2} | \langle l_2 m_{l2} | \langle s_1 m_{s1} | \hat{\mathcal{H}}_{\text{dip}} | s_1 m'_{s1} \rangle | l_2 m'_{l2} \rangle | s_2 m'_{s2} \rangle | L' M'_L \rangle \\
&= -\sqrt{30} \delta_{m_{l2} m'_{l2}} \lambda_{s1s2}(R) (-1)^{s_1 - m_{s1} + s_2 - m_{s2} - M_L} [s_1(s_1+1)(2s_1+1)s_2(s_2+1)(2s_2+1)(2L+1)(2L'+1)]^{1/2} \\
&\quad \times \begin{pmatrix} L & 2 & L' \\ 0 & 0 & 0 \end{pmatrix} \sum_{q_1, q_2} \begin{pmatrix} 1 & 1 & 2 \\ q_1 & q_2 & -q \end{pmatrix} \begin{pmatrix} s_1 & 1 & s_1 \\ -m_{s1} & q_1 & m'_{s1} \end{pmatrix} \begin{pmatrix} s_2 & 1 & s_2 \\ -m_{s2} & q_2 & m'_{s2} \end{pmatrix} \begin{pmatrix} L & 2 & L' \\ -M_L & -q & M'_L \end{pmatrix} \\
&\quad -\sqrt{30} \delta_{m_{s2} m'_{s2}} \lambda_{s1l2}(R) (-1)^{s_1 - m_{s1} + l_2 - m_{l2} - M_L} [s_1(s_1+1)(2s_1+1)l_2(l_2+1)(2l_2+1)(2L+1)(2L'+1)]^{1/2} \\
&\quad \times \begin{pmatrix} L & 2 & L' \\ 0 & 0 & 0 \end{pmatrix} \sum_{q_1, q_2} \begin{pmatrix} 1 & 1 & 2 \\ q_1 & q_2 & -q \end{pmatrix} \begin{pmatrix} s_1 & 1 & s_1 \\ -m_{s1} & q_1 & m'_{s1} \end{pmatrix} \begin{pmatrix} l_2 & 1 & l_2 \\ -m_{l2} & q_2 & m'_{l2} \end{pmatrix} \begin{pmatrix} L & 2 & L' \\ -M_L & -q & M'_L \end{pmatrix}, \tag{A10}
\end{aligned}$$

with the  $R$ -dependent spin-spin coupling  $\lambda_{s1s2}(R) = E_h \alpha^2 a_0^3 / R^3$  ( $\alpha \approx 1/137$  is the fine-structure constant),  $\lambda_{s1l2} = (g'_L/g_S) \lambda_{s1s2}$  and  $q \equiv q_1 + q_2$ . In the  $ls$ -coupled basis set,

$$\begin{aligned}
& \langle LM_L | \langle (l_2 s_2) j_2 m_{j2} | \langle s_1 m_{s1} | \hat{\mathcal{H}}_{\text{dip}} | s_1 m'_{s1} \rangle | (l_2 s_2) j'_2 m'_{j2} \rangle | L' M'_L \rangle \\
&= \sqrt{30} (-1)^{s_1 - m_{s1} + j_2 + l_2 + s_2 - m_{j2} - M_L} [s_1(s_1+1)(2s_1+1)(2j_2+1)(2j'_2+1)(2L+1)(2L'+1)]^{1/2} \begin{pmatrix} L & 2 & L' \\ 0 & 0 & 0 \end{pmatrix} \\
&\quad \times \left[ \lambda_{s1s2}(R) (-1)^{j_2} [s_2(s_2+1)(2s_2+1)]^{1/2} \begin{Bmatrix} s_2 & j'_2 & l_2 \\ j_2 & s_2 & 1 \end{Bmatrix} + \lambda_{s1l2}(R) (-1)^{j'_2} [l_2(l_2+1)(2l_2+1)]^{1/2} \begin{Bmatrix} l_2 & j'_2 & s_2 \\ j_2 & l_2 & 1 \end{Bmatrix} \right] \\
&\quad \times \sum_{q_1, q_2} \begin{pmatrix} 1 & 1 & 2 \\ q_1 & q_2 & -q \end{pmatrix} \begin{pmatrix} s_1 & 1 & s_1 \\ -m_{s1} & q_1 & m'_{s1} \end{pmatrix} \begin{pmatrix} j_2 & 1 & j_2 \\ -m_{j2} & q_2 & m'_{j2} \end{pmatrix} \begin{pmatrix} L & 2 & L' \\ -M_L & -q & M'_L \end{pmatrix}. \tag{A11}
\end{aligned}$$

These expressions show that  $\hat{\mathcal{H}}_{\text{dip}}$  adds to the couplings produced by  $\hat{V}$  in that: (1) it relaxes the constraint of  $M_S$  being conserved, as long as  $\Delta M_S = -\Delta M_L$ ; and (2) it allows for changes in  $m_{l2}$  that preserve  $M_L$ . The 3- $j$  symbols in Eqs. (A8)–(A11) restrict  $\Delta L$  to be even, and thus channels with only even (or only odd)  $L$  values appear in the basis set for a given total parity  $P$ .

---